Experimental Investigations on Thermal Performance of Closed-Loop Pulsating Heat Pipe using Machine Learning

Kamlesh Parmar, Nirmal Parmar, Ajit Kumar Parwani, and Sumit Tripathi

October 21, 2023

Abstract

In a wide range of thermal applications, Pulsating Heat Pipes (PHP) have shown to be adaptable and effective thermal solutions. In the present paper, extensive experimental study was conducted on the PHP's thermal performance improvement by using conventional and nanofluids as heat transfer fluid at different filling ratios and heat inputs. Furthermore, data analysis and machine learning were used to find best thermal parameter and to predict low thermal resistance for PHP.

During series of experiments, two different heat transfer fluids; deionized (DI) water and nanofluid (Al_2O_3-DI water 0.1wt.%) were used. Firstly, experiments were conducted at specific temperature and pressure to estimate a filling ratio with the lowest possible thermal resistance. To achieve this goal, experiment were conducted at four different filling ratios such as 20%, 40%, 60%, and 80% at constant heat input of 80 W. In the second stage, experiments were conducted with various heat inputs such as 40 W, 60 W, 80 W, 100 W, and 120 W with a constant filling ratio. The generated experimental data were used to prepare data driven solution, specifically data analysis and machine learning. A dedicated python library named PyPulseHeatPipe was created to perform statistical analysis and data visualization. In addition to that, to predict the optimal thermal resistance for given thermal parameter such as filling ration, heat transfer fluid, and temperature machine learning solution was conducted. The trained machine learning model has capability to predict thermal resistance with XX% accuracy. These study put efforts towards establishing the groundwork for more effective utilization of PHPs in diverse engineering systems by fusing experimental work with data-driven solution.

1 Introduction

The pulsating heat pipe (PHP) is two-phase passive thermal device which was invented by H. Akachi in 1990 [2] and small-sized meandering tube as shown in Figure 1. PHPs are belongs to the thermal system category of heat pipes. PHPs are used to transfer heat from a hot source to a cold source by pulsating the liquid-vapor system effectively [11]. PHP has a wide range of thermal applications since last two decades such as avionic and space, waste heat recovery [7], electric vehicle battery cooling [4, 28, 33], renewable energy applications, electronics device cooling [3, 7], heat ex-changers, cryogenics, pv cooling, solar collectors, solar water systems and fuel cell cooling [4, 19].

Table 1: **List of Conventional fluids studied in literature of PHPs**

Conventional fluids	**Properties**			
	TR	**dT**	**Q**	**FRs**
Water	[5, 9, 11, 21, 26, 28]		[9, 11, 21, 26, 28]	[5, 9, 11, 26, 28]
Dionized water (DI)	[14, 21, 27]		[14, 21, 27]	[27]
Acetone	[5, 12, 20, 21]		[12, 20, 21]	[5, 12]
Ethanol	[5, 9, 11, 14, 18, 21, 28, 32]	[18]	[9, 11, 14, 18, 21, 28, 32]	[5, 9, 28, 32]
Methanol	[21]		[21]	
R-134a	[11]		[11]	
R-123	[9, 10]		[9, 10]	[9, 10]

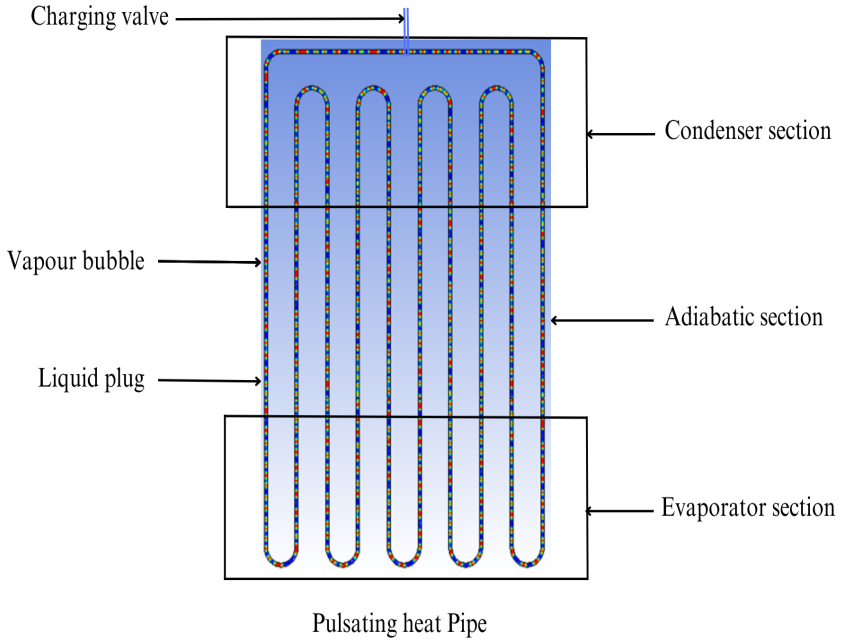

Figure 1: Schematic of the PHPs

As per the literature review of PHPs, the use of various convectional fluids as working fluids are not new to enhance the thermal performance of PHPs as shown in Table 1. Water and ethanol are widely used as conventional fluids to increase heat transfer capability of PHP as shown as Table 1. In addition to this, the use of various nanofluids as working fluids are also not newer to increase the thermal performance of PHPs as shown in Table 2.

The working parameters of the PHPs are categorized into three groups to determine heat transfer capability [7]: (a) Geometric working parameters (b) Physical properties of working fluids and (c) Operational parameters. In majority of literature, the thermal performance of PHPs reported by considering a thermal resistance, temperature difference between evaporator and condenser, heat inputs and filling ratios for conventional fluids and nanofluids as thermal performance parameters which is shown in Table 1 and 2.

Table 2: **List of Nanofluids studied in literature of PHPs**
(TR - Thermal resistance, dT - Temperature difference, Q - Heat input and FRs - Filling ratios)

Nanofluids		**Concentration**	**Properties**			
Nanoparticles	**Base fluids**		**TR**	**dT**	**Q**	**FRs**
TiO_2	Water	2vol%	[4]	[4]	[4]	
Graphene	Water-ethylene glycol	0.1-1 mg/ml	[12]		[12]	[12]
Graphene	Ethanol-water mixture	0.1-1 mg/ml	[31]		[31]	
Diamond	Water	1vol%	[16]	[16]		
Al_2O_3	Water	0-1.2wt.%	[23]		[23]	
Al_2O_3	Pure water	1-4vol%		[25]	[25]	
Al_2O_3	Water	0-1.2wt.%	[24]		[24]	[24]
Al_2O_3	Pure water	0-2vol%		[8]	[8]	
SiO_2	Water	0-0.6wt.%	[23]		[23]	
CuO	Pure water	0-2vol%		[8]	[8]	
MWCNs	Water-ethanol	0.05-0.5wt.%	[34]	[34]	[34]	
MWCNs	Pure water	0-1wt.%	[29]	[29]	[29]	
Al_2O_3-CuO	Water	0.1wt.%	[35]		[35]	
SiO_2-CuO	Water	0.1wt.%	[35]		[35]	
Ferrofluid	Distilled water	2.5 and 7vol%	[17]		[17]	[17]
Silver	Pure water	0-2vol%		[8]	[8]	
Silver	Water	100 and 450 ppm	[13]	[13]	[13]	[13]
Silver	Water	0.25-1vol%	[30]		[30]	[30]

In this present work, initially the thermal resistance, various filling ratios and temperature difference between evaporator and condenser at constant heat input and various heat inputs were considered to analyze the thermal performance of closed loop pulsating heat pip (CLPHP). After the experiments, the data analysis of CLPHP has been done and came to know that the thermal resistance, temperature difference between evaporator and condenser, heat inputs and filling ratios are good to understand the thermal performance of CLPHPs but they are not sufficient as thermal parameters to understand thermal performance of PHPs.

The experiments were conducted on closed loop pulsating heat pipe (CLPHP) with two filling ratios (40% and 60%) and two charging fluids (DI water and Al_2O_3-DI water nanofluid of 0.1wt.% nanoparticles). In presented paper, the statistical analysis was performed and calculated Expanded Uncertainty (EU) to understand a characteristics of CLPHP.

The PyPulseHeatPipe Python library here was prepared to calculate the behaviour and characteristics of given CLPHP. Addition to this, Module for Advanced data analysis and Machine learning model here have been done for CLPHP by considering the thermal resistance, filling ratios and temperature difference between evaporator and condenser at constant and various heat inputs using two working fluids.

2 Experimental Setup

The entire experimental setup of CLPHP was constructed at the Heat and Mass Transfer Laboratory, Institute of Infrastructure Technology Research and Management (IITRAM), Ahmedabad, India.

2.1 Experimental setup description

The given CLPHP has evaporator section at bottom in which heat is received and the heat is dissipated in the condenser section. There is a part between an evaporator and a condenser section, which is called the adiabatic section as shown in Figure 2. The CLPHP has three sections those are condenser, adiabatic and evaporator sections. The adiabatic, evaporator, and condenser section's lengths can be changed as requirement. Level screws are used to level the arrangement. In order to cool the CLPHP, natural convection is utilised. The condenser section was open to atmosphere. The adiabatic section of CLPHP is covered by the thick glass wool with aluminium foil that effectively insulates to reduce heat loss below the condenser section. The CLPHP is a closed-loop device with only one pressure gauge and one charging valve. With the aid of the provided syringe and valve, a vacuum was created inside CLPHP and working fluids ware charged.

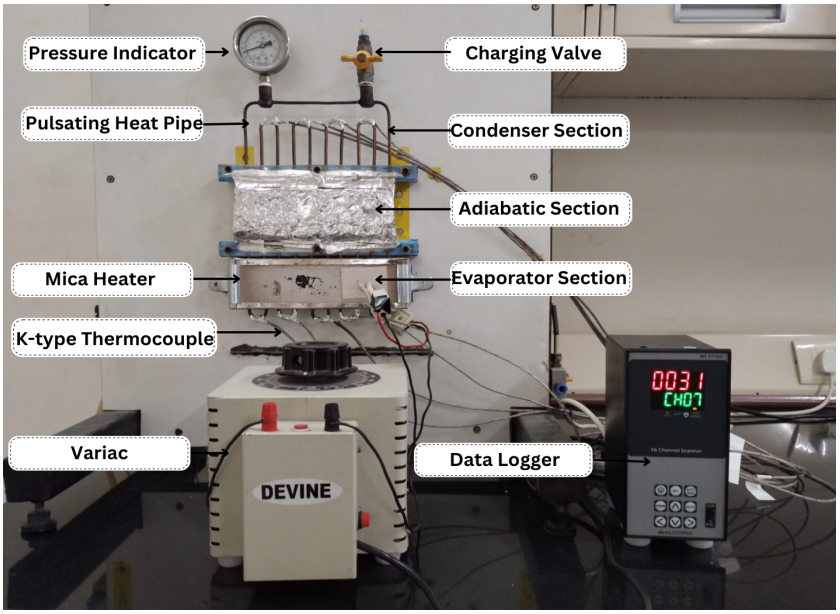

Figure 2: Pulsating heat pipe experimental setup

The given CLPHP using a vertical orientation of 5 turns, depicted has an overall width of 183.5 mm and a height of 282.3 mm. Long capillary copper tubes measuring a diameter of 2.15 mm on the inside and 4.15 mm on the outside were used to construct the CLPHP. The bending radius of CLPHP is 9 mm. Two mica heater (each 400 W at 230 V; max: 400° C, 200 mm x 60 mm) was used to apply the thermal load in the evaporator section. In addition, a variable transformer (variac) is utilized to maintain a constant heat supply. There are no such heat losses as glass wool was used as insulation at adiabatic section.

The K-type thermocouples were used to measure temperatures of evaporator and condenser sections by using 16 channel scanner with USB data logger RS-485 communication (Multispan, MS-5716 RU-M1). Each thermocouple has attached to data logger. The condenser section of the CLPHP was equipped with four thermocouples (T_1, T_2, T_3 and T_4) and the evaporator section loops with five thermocouples (T_5, T_6, T_7, T_8 and T_9) as shown in Figure 2. A variac was utilized to control the voltage supply. The accuracy of various measuring instruments is given below in Table 3.

Table 3: **The accuracy of various measuring instruments**

Sr.No.	Measuring instrument	Accuracy
1	Mica heater	± 0.5° C
2	Thermocouple	± 1.0 %
3	Steel ruler	± 1.0 mm
4	Syringe	± 1.0 ml

2.2 Preparation of Al_2O_3-DI water nanofluid

The Al_2O_3 nanoparticles size of 10 nm were collected from in-house at the Physics laboratory of IITRAM. 0.1wt.% Al_2O_3 nanoparticles [24] with DI water as base fluid and Surfactants are used for preparation of Al_2O_3-DI water nanofluid. The settlement of nanoparticles mostly collected at evaporator section [24]. Hence, Sodium Dodecyl Sulphate (SDS) surfactant [6] (mass ratio of 2:1 for SDS particle) is utilized to suspend Al_2O_3 nanoparticles in DI water. The preparation of Al_2O_3-DI water nanofluid was conducted at the Physics laboratory of IITRAM.

2.3 Experimental procedure

Initially, an evaporator was heated by mica heater to remove unwanted previously used fluids or gases. A vacuum pressure of 160 mm of Hg (0.2133 bar) was created with the help of a syringe during each experiments and working fluid was filled through a charging valve. The temperatures of evaporator and condenser sections were measured by using 16 channel scanner with USB data logger RS-485 communication (Multispan, MS-5716 RU-M1).

The experimental data of CLPHP were collected by using DI water and filling ratios (40% and 60%) at constant heat input of 80 W and various heat inputs (40 W to 120 W) at 60% FR. Similarly, the experimental data were collected by using Al_2O_3-DI water nanofluid and filling ratios (40% and 60%) at constant heat input of 80 W and various heat inputs (40 W to 120 W) at 60% FR. These experiments repeated for four times to check its repeatability and reproducibility. The series of experiments were conducted and collected the data of CLPHP. A sets of experiments on CLPHP setup were performed to measure pressure, temperature of evaporator and condenser section. The data were collected through Multispan temperature scanner and data logger in each 30 sec during each experiments.

The heat transfer capability of PHP measured by the thermal resistance that is calculated by

$TR = \frac{(T_e - T_c)}{Q}$

where T_e and T_c denote the average temperature evaporator section and condenser section respectively. Q is a heat input by a heater at evaporator section.

$T_c = \frac{1}{4}\sum_{i=1}^{4} T_i$

$T_e = \frac{1}{5}\sum_{i=5}^{9} T_i$

where T_i (i=1 to 9) are surface temperature of PHP wall which were measured by k-type thermocouples as shown in fig 2.

2.4 Machine learning prediction for CLPHP

The area of machine learning is a fast-developing discipline enabled based on data optimization [15]. The decision-tree-based foundation of the random forest technique involves dividing the data into several branches based on distinct subsets of the data. Several decision trees are built using the random forest method, and the characteristics are also randomly chosen [1]. This method is unique in that it identifies and ranks the data-sets most pertinent features in relation to the categorical replies. This can be helpful as an addition to the research on how individual features affect output response. The primary drawback of this technique is the lengthy computing time needed for implementation, which goes up as there are more trees to construct [22].

3 Results and Discussion

3.1 Analysis of a PHP at constant heat input with different filling ratios

After the performing the four sets of experiments, the series of experiments data were analysed for two working fluids (DI water and Al_2O_3-DI water nanofluid using 0.1wt.% nanoparticles) and two filling ratios (40% and 60%) at a constant heat input of 80 W. The nanoparticles can increased a heat transfer capability of the PHP as compared with the pure water. The nanoparticles were suspended in the base fluid due to pulsation and movements of working fluid [16]. The nanoparticles agglomeration were observes at both condenser and evaporator section. Nevertheless, the nanoparticles settlement was more at evaporator section as compared to condenser section [24]. To enhance the suspension of Al_2O_3 nanoparticles with the base fluid of DI water, SDS surfactant were used which decrease the agglomeration of nanoparticles near evaporation section [6].

Due to good insulation at adiabatic section, the heat loss from adiabatic section to atmosphere was very less. In the presented paper, the statistical analysis was calculated and plotted with an Expanded uncertainty (EU) with 95% of significance level to understand a characteristics of CLPHP for all sets of experimental results.

From the literature, it is observed that the thermal performance of PHP is the function of pressure inside PHP and temperature of condenser and evaporator section. Due to a constant heat input during all the experiments of current section, the variations of average temperature of condenser, pressure and thermal resistance were plotted with respect to average temperature of evaporator. The thermal resistance was computed by using given equation of it. From the literature, it is observed that, thermal resistance is a only thermal parameter to understand heat transfer enhancement characteristics of the PHPs as shown in the Table 1 and Table 2.

The variation of temperature of condenser with respect to temperature of evaporator at a heat input of 80 W for DI water and Al_2O_3-DI water nanofluid were plotted by considering 40% filling ratio as shown in figure 3. The regression lines of both fluids is plotted and calculated with 95% of Expanded Uncertainty. The plot is also included the experimental data and average value of temperatures. It is clearly visible in figure 3 that the trends for temperature of evaporator and condenser were followed for all sets of experiments for both the working fluids and no change variations of temperature for DI water and nanofluid for 40% FR. Hence, the repeatability of given PHP setup is quiet good. At initial stage of experiments, temperature of condenser is increased quicker than nanofluid. However, the inflation of an evaporator temperature was occurred near about 330 K to 355 K. After that, the temperature of condenser is reduced for nanofluid as compare to DI water.

The figure 4 is represented the variation of pressure with respect to temperature of evaporator at a heat input of 80 W for DI water and Al_2O_3-DI water nanofluid by considering 95% of Expanded Uncertainty with 40% filling ratio. The pressure of PHP is initially decreased then it is increased for entire experiment. Where as the pressure of DI water is continuously increased from beginning of experiment. The slope of a pressure for PHP using nanofluid is lesser than DI water above 345 K. It is observed that the Expanded Uncertainty for pressure is increased at higher temperature of evaporator (above 355 K) because of the containment of nanoparticles volume is higher in liquid slugs. The plotted graph clearly shown that the thermal performance of PHP works better under the vacuum conditions.

The variation of thermal resistance with respect to temperature of evaporator at a heat input of 80 W for DI water and Al_2O_3-DI water nanofluid are plotted as shown in figure 5 and calculated with 95% of Expanded Uncertainty using 40% filling ratio. The thermal resistance of given PHP

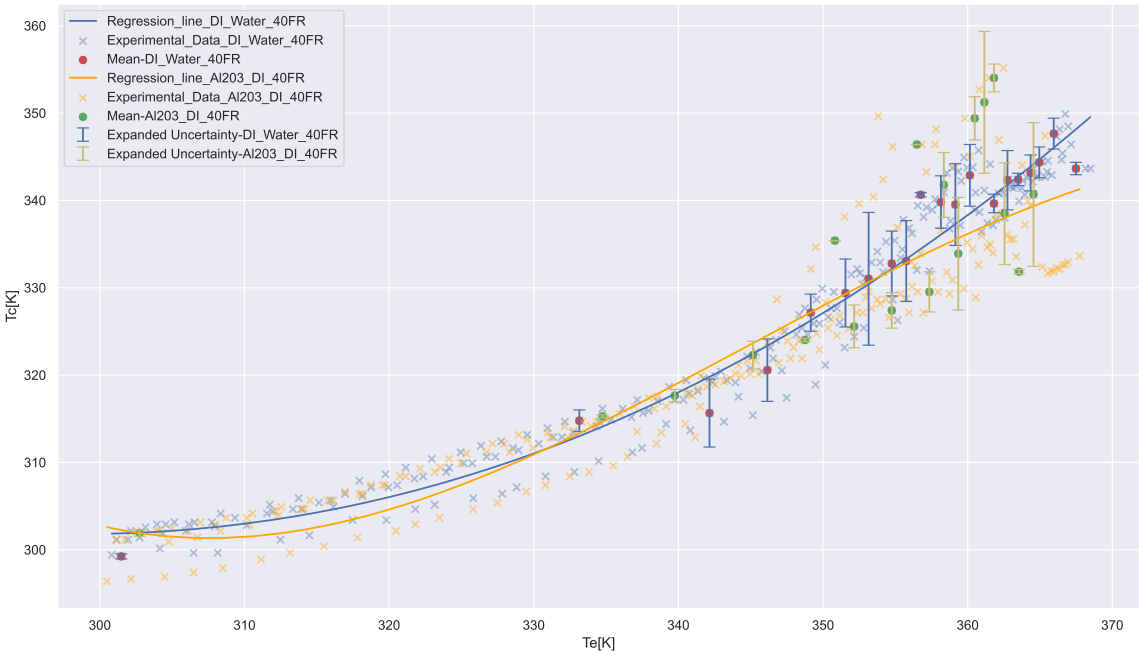

Figure 3: Variation of temperature of condenser with respect to temperature of evaporator at a heat input of 80 W for 40% FR (Working fluids :- DI water and Al_2O_3-DI water nanofluid using 0.1wt.%)

is lesser between evaporator temperature of 330 K to 355 K using nanofluid. In addition to this, the thermal resistance is increased above 355 K because of higher nanoparticles volume contained in liquid slug as compared to bubbles. So as a results, the expanded uncertainty is more at higher temperature of evaporator above 355 K. While increasing the temperature of evaporator, the thermal resistance was increased in proper tends up to 345 K and afterthought, PHP was behaved unpredictable due to stagger data density.

The variation of temperature of condenser with respect to temperature of evaporator at a heat input of 80 W for DI water and Al_2O_3-DI water nanofluid are plotted as shown in figure 6 by considering 60% filling ratio with 95% of Expanded Uncertainty. It is clearly visible in figure 6 that the trends for temperature of evaporator and condenser are followed for all sets of experiments for both the working fluids. At initial stage of experiments, temperature of condenser is increased higher than nanofluid. However, the inflation of an evaporator temperature was occurred near about 330 K. Similarly, the repeatability of given PHP setup is also quiet good while using 40% and 60% filling ratios.

The figure 7 is represented the variation of pressure with respect to temperature of evaporator at a heat input of 80 W for DI water and Al_2O_3-DI water nanofluid by considering 95% of Expanded Uncertainty with 60% filling ratio. The trend of both the fluids were similar while the thermal performance of the nanofluids is stable. The plotted graph clearly shown that the thermal performance of PHP works better under the vacuum conditions.

The variation of thermal resistance with respect to temperature of evaporator at a heat input of 80 W for DI water and Al_2O_3-DI water nanofluid are plotted as shown in figure 8 with 95% of Expanded Uncertainty using 60% filling ratio. It is observed that the thermal resistance was nearly similar for both the working fluids up to temperature of evaporator about 320 K or 330 K. Where as above 320 K or 330 K, thermal resistance of PHP is lesser for nanofluid compare to DI water. When the evaporator temperature is increased above 345 K, something is going on inside PHP related to thermal thermal performance which is nearer to atmospheric pressure. In addition, while increasing the temperature of evaporator, the thermal resistance was increased in proper tends up to 345 K and afterthought, PHP was behaved unpredictable due to stagger data density.

The Table 4 shows the details of thermal parameters of PHP for two working fluids at different FRs at 80 W which includes the average value and Expanded Uncertainty of thermal parameters.

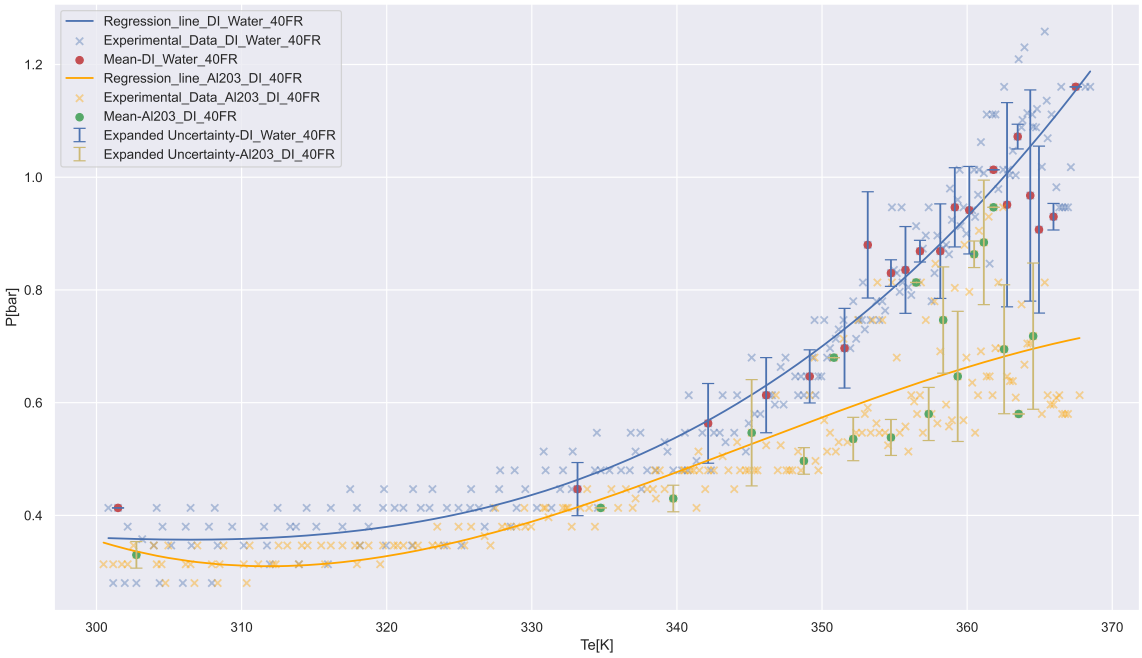

Figure 4: Variation of pressure with respect to temperature of evaporator at a heat input of 80 W for 40% FR (Working fluids :- DI water and Al_2O_3-DI water nanofluid using 0.1wt.%)

3.2 Analysis of a PHP at different heat inputs with constant filling ratio

From section 3.1, it is noted that the filling ratio of 60% is better than other used filling ratios in current experiment work (Include citations). Therefore, the constant filling ratio of 60% is used at different heat inputs (40 W to 120 W) in the experiments of PHP using DI water and Al_2O_3-DI water nanofluid (NF) using 0.1wt.% nanoparticles and discussed in this section.

As shown figure 9, the comparison of variation for regression lines of condenser temperature with respect to evaporator temperature at various heat inputs using DI water and Al_2O_3-DI water nanofluid (NF) were plotted by considering 60% filling ratio. The regression lines showcased similar trends for all the condenser and evaporator temperatures. It is observed that condenser temperatures for NF were higher compared to DI water at respective given heat inputs. The average values of condenser temperature and Expanded Uncertainty (EU) were calculated and shown in the Table 5 at different heat inputs. Table 6 is shown the coefficients of regression for condenser temperature in the order of 3rd degree of polynomial equation at different heat inputs.

The figure 10 is represented the variation for regression lines of pressure with respect to evaporator temperature at various heat inputs for DI water and Al_2O_3-DI water nanofluid with 60% filling ratio. It is noted that the pressure for nanofluid is higher compared to DI water at heat inputs of 40 W and 120 W. However, It is observed that the pressure for nanofluid is lesser compared to DI water at heat inputs of 60 W, 80 W and 100 W. The average values of pressure and Expanded Uncertainty (EU) were calculated and shown in the Table 5 at different heat inputs. Table 6 is shown the coefficients of regression for pressure in the order of 3rd degree of polynomial equation for different heat inputs.

As shown in figure 11, The comparison of variation for regression lines of thermal resistance with respect to evaporator temperature are plotted at various heat inputs for DI water and Al_2O_3-DI water nanofluid using 60% filling ratio. It is observed that the thermal resistance is decreased compare to DI water for all the given heat inputs (add citations). For both the working fluids, it is noted that when the heat inputs increased then the thermal resistance is reduced (add citations). The average values of thermal resistance and Expanded Uncertainty (EU) were calculated and shown in the Table 5 for different heat inputs. Table 6 shown the coefficients of regression for pressure in the order of 3rd degree for polynomial equation for different heat inputs.

The variation of thermal resistance with respect to heat input for DI water and Al_2O_3-DI water nanofluid (NF) are plotted with 95% of Expanded Uncertainty as shown in figure 12 using 60% filling ratio.It is observed the thermal resistance is decreased by increasing the heat inputs. The trends of DI water and nanofluid were parallel to each other.

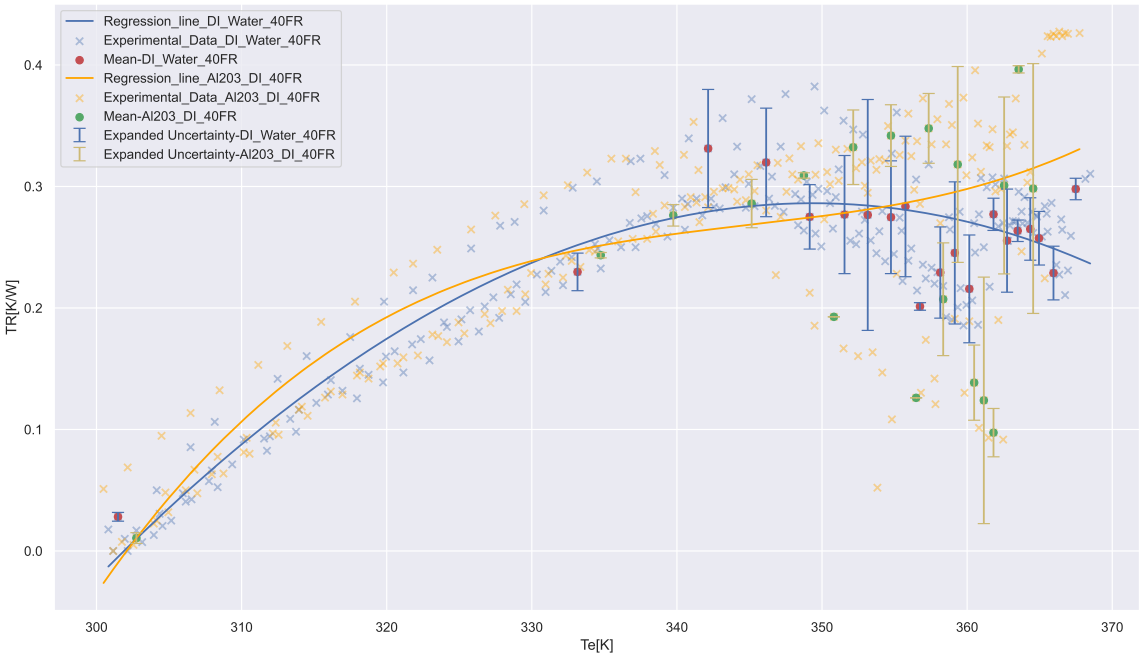

Figure 5: Variation of thermal resistance with respect to temperature of evaporator at a heat input of 80 W for 40% FR (Working fluids :- DI water and Al_2O_3-DI water nanofluid using 0.1wt.%)

The Table 5 shows the details of thermal parameters of PHP at different heat inputs with constant filling ratio of 60% which includes the average value and Expanded Uncertainty of thermal parameters.

The Table 6 shows the details of regression coefficients for thermal parameters of PHP for two working fluids using different FRs at constant heat input of 80 W. Where a_0, a_1, a_2 and a_3 are coefficients of regression.

The Table 7 shows the details of regression coefficients for thermal parameters of PHP for DI water using 60% FRs at various heat inputs. Where a_0, a_1, a_2 and a_3 are regression coefficients.

The Table 8 shows the details of regression coefficients for thermal parameters of PHP for nanofluid using 60% FRs at various heat inputs. Where a_0, a_1, a_2 and a_3 are regression coefficients.

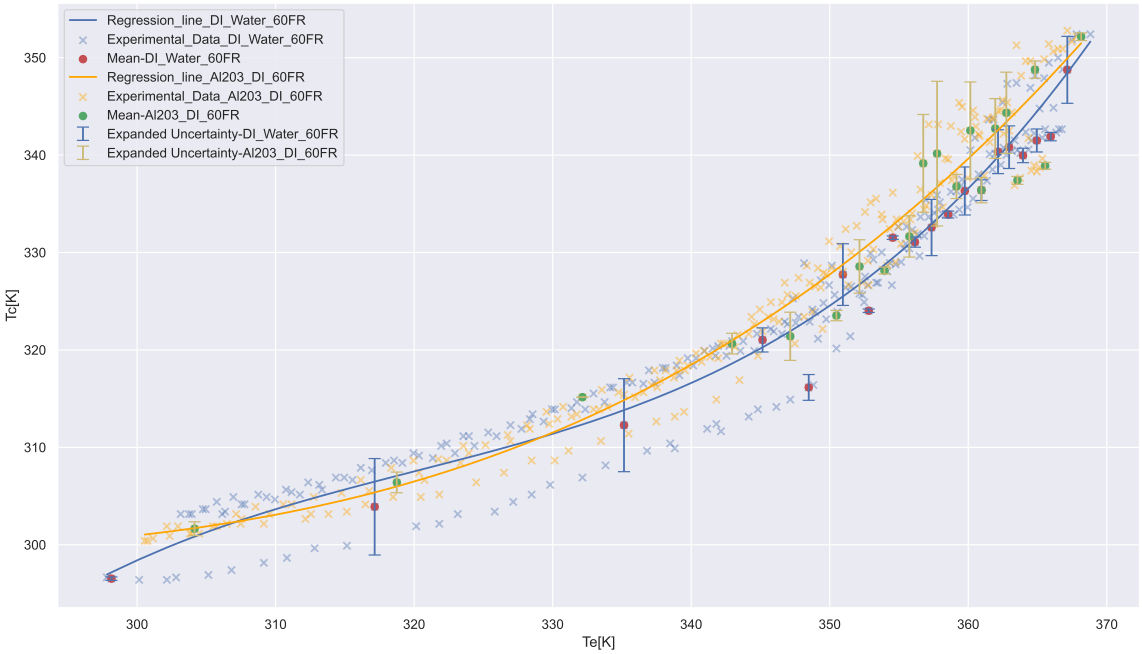

Figure 6: Variation of temperature of condenser with respect to temperature of evaporator at a heat input of 80 W for 60% FR (Working fluids :- DI water and Al_2O_3-DI water nanofluid using 0.1wt.%)

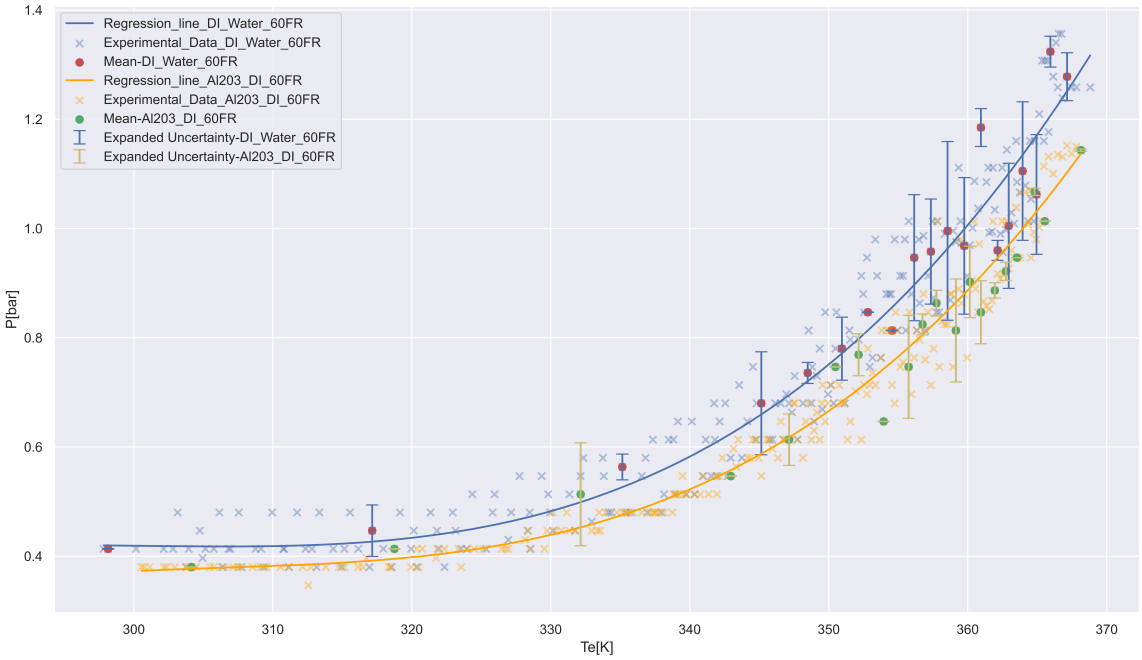

Figure 7: Variation of pressure with respect to temperature of evaporator at a heat input of 80 W for 60% FR (Working fluids :- DI water and Al_2O_3-DI water nanofluid using 0.1wt.%)

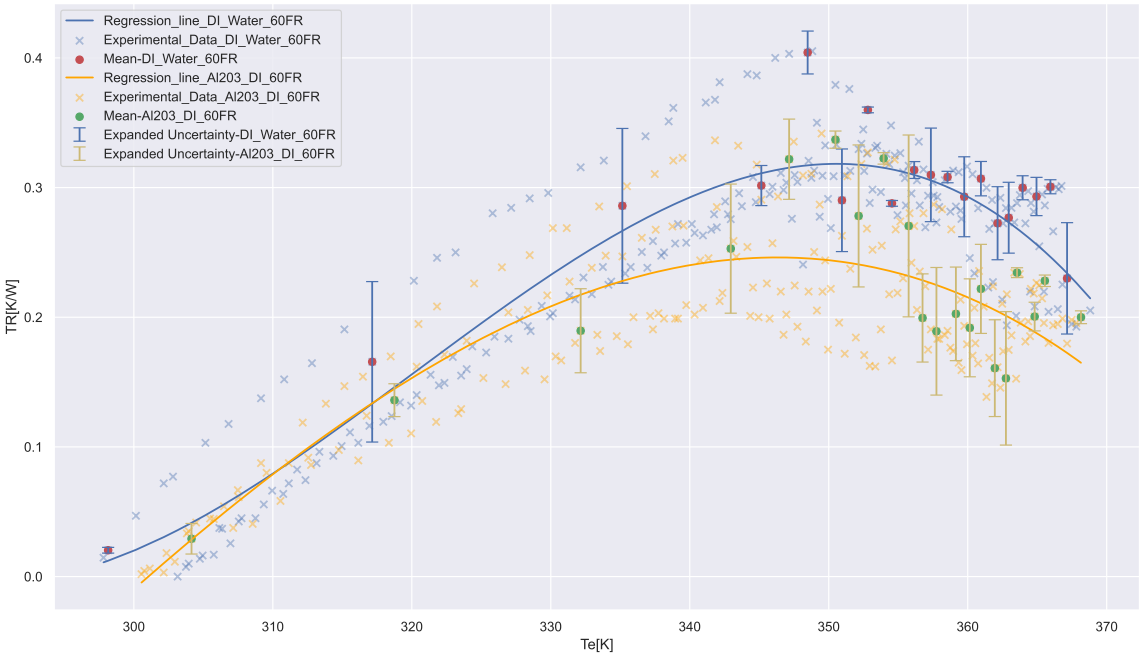

Figure 8: Variation of thermal resistance with respect to temperature of evaporator at a heat input of 80 W for 60% FR (Working fluids :- DI water and Al_2O_3-DI water nanofluid using 0.1wt.%)

Table 4: **Details of thermal parameters of PHP for two working fluids at different FRs at 80 W**

Thermal parameters	**Working fluids**	**FRs[%]**	**Average**	**EU**
T_c [K]	DI water	40%	309.5242	1.7149
		60%	309.8712	0.9849
	NF (0.1 wt.%)	40%	309.17	0.8405
		60%	310.7738	0.8281
P [bar]	DI water	40%	0.4309	0.0381
		60%	0.4886	0.0277
	NF (0.1 wt.%)	40%	0.3827	0.0175
		60%	0.4481	0.0136
dT [K]	DI water	40%	14.7393	1.7149
		60%	15.0737	0.9849
	NF (0.1 wt.%)	40%	15.3957	0.8405
		60%	13.5965	2.0844
TR [K/W]	DI water	40%	0.1842	0.0214
		60%	0.1884	0.0123
	NF (0.1 wt.%)	40%	0.1924	0.0105
		60%	0.17	0.0261

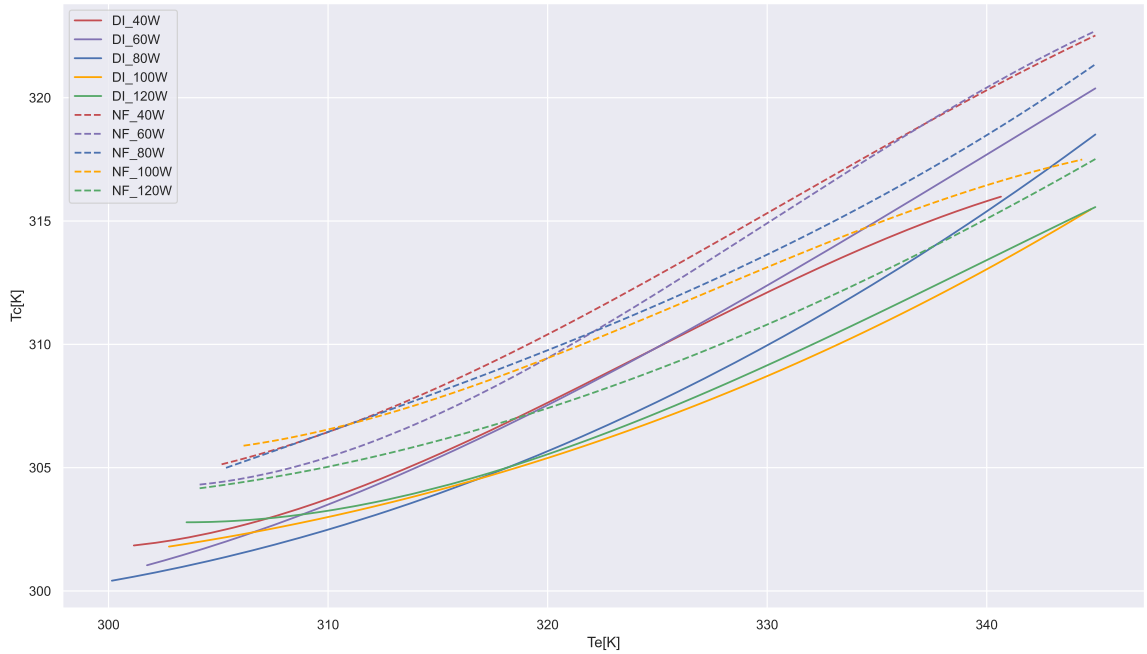

Figure 9: Comparison of variation for regression lines of condenser temperature with respect to evaporator temperature using 60% FR (Heat inputs:- 40 W, 60 W, 80 W, 100 W and 120 W, Working fluids :- DI : DI water and NF: Al_2O_3-DI water nanofluid using 0.1wt.%)

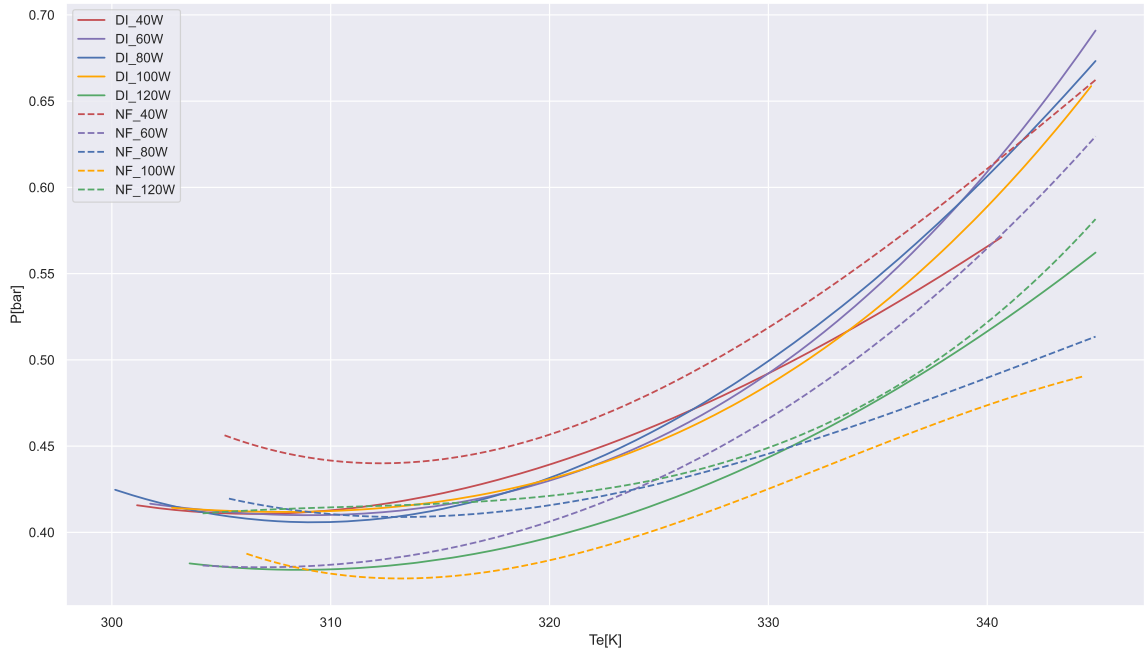

Figure 10: Comparison of variation for regression lines of pressure with respect to evaporator temperature using 60% FR (Heat inputs:- 40 W, 60 W, 80 W, 100 W and 120 W, Working fluids :- DI : DI water and NF: Al_2O_3-DI water nanofluid using 0.1wt.%)

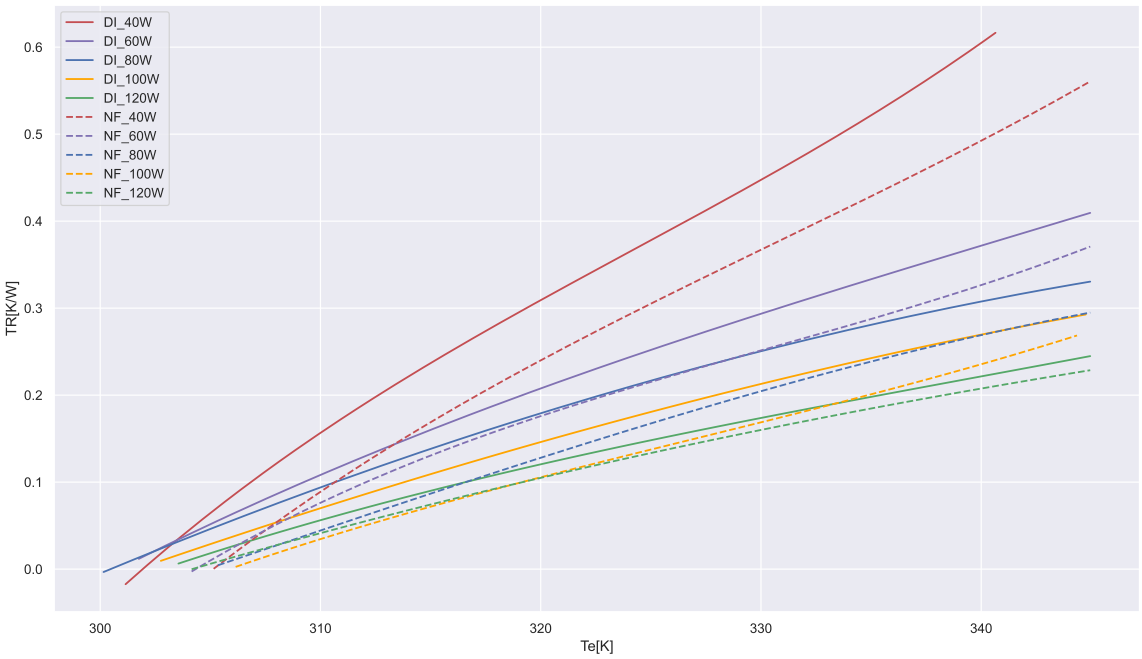

Figure 11: Comparison of variation for regression lines of thermal resistance with respect to evaporator temperature using 60% FR (Heat inputs:- 40 W, 60 W, 80 W, 100 W and 120 W, Working fluids :- DI : DI water and NF: Al_2O_3-DI water nanofluid using 0.1wt.%)

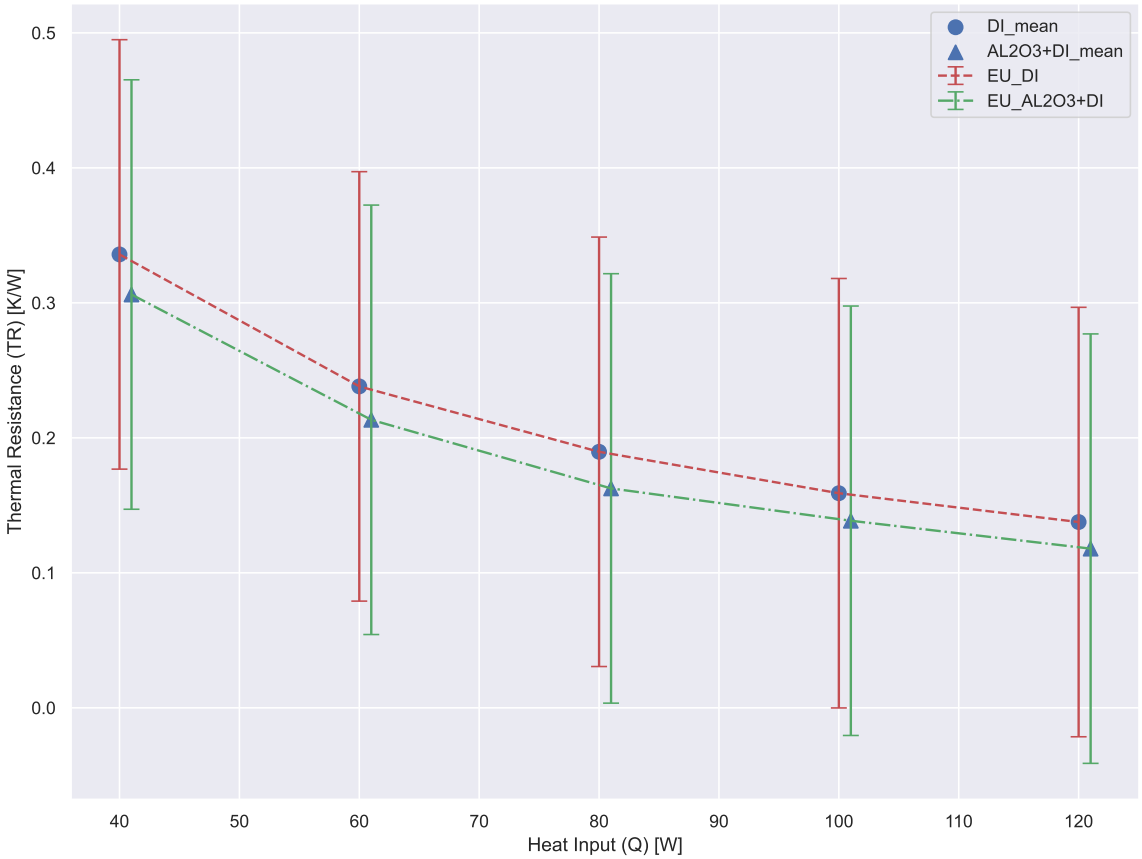

Figure 12: Variation of thermal resistance with respect to heat input for DI water and Al_2O_3-DI water nanofluid using 60% FR (EU:- Expanded Uncertainty, Working fluids :- DI : DI water and NF: Al_2O_3-DI water nanofluid using 0.1wt.%)

Table 5: **Details of thermal parameters of PHP for two working fluids at different heat inputs with FR of 60%**

Thermal parameters	**Heat inputs Q[W]**	**Average**		**EU**	
		DI water	**NF (0.1wt.%)**	**DI water**	**NF (0.1wt.%)**
T_c [K]	40 W	308.8523	313.5461	0.1218	0.1539
	60 W	310.1953	316.4905	0.0908	0.238
	80 W	307.8108	324.4682	0.1608	1.1988
	100 W	307.0462	334.6406	0.5596	2.0863
	120 W	307.8161	332.2857	0.2	4.2646
P [bar]	40 W	0.4652	0.5144	0.0013	0.001
	60 W	0.4905	0.5196	0.0014	0.0022
	80 W	0.4837	0.6081	0.0017	0.016
	100 W	0.4754	0.7664	0.0143	0.025
	120 W	0.4355	0.8291	0.0000	0.0936
dT [K]	40 W	13.4358	12.3039	0.1218	0.1539
	60 W	14.2872	14.9776	0.091	0.238
	80 W	15.1734	14.5542	0.161	1.1988
	100 W	15.8982	14.2946	0.560	2.0863
	120 W	16.5155	14.9744	0.200	4.2646
TR [K/W]	40 W	0.3359	0.3076	0.0030	0.0038
	60 W	0.2381	0.2496	0.0015	0.004
	80 W	0.1897	0.1819	0.0020	0.015
	100 W	0.159	0.1429	0.0056	0.0209
	120 W	0.1376	0.1248	0.0017	0.0355

Table 6: **Details of regression coefficients for thermal parameters of PHP for two working fluids using different FRs at constant heat input of 80 W**

Thermal parameters	Working fluids	FRs[%]	a_0	a_1	$a_2 \times 10^{-3}$	$a_3 \times 10^{-5}$
T_c [K]	DI water	40%	0.00	-2.6148	-0.3122	1.0467
		60%	0.00	70.3436	-218.6320	22.7685
	NF (0.1 wt.%)	40%	0.00	-74.4540	218.3611	-21.0952
		60%	0.00	12.3817	-45.4785	5.5795
P [bar]	DI water	40%	0.00	0.4749	-1.6477	0.1899
		60%	0.00	0.7976	-2.6512	0.2937
	NF (0.1 wt.%)	40%	0.00	-1.0353	3.0271	-0.2923
		60%	0.00	0.8306	-2.7111	0.2953
dT [K]	DI water	40%	0.00	3.6148	0.3122	-1.0467
		60%	0.00	-69.3436	218.6320	-22.7685
	NF (0.1 wt.%)	40%	0.00	75.4540	-218.3611	21.0952
		60%	0.00	-13.0464	49.9932	-5.9978
TR [K/W]	DI water	40%	0.00	0.0453	0.0036	0.0131
		60%	0.00	-0.8668	2.7329	-0.2846
	NF (0.1 wt.%)	40%	0.00	0.9432	-2.7295	0.2637
		60%	0.00	-0.1631	0.6249	-0.0750

Table 7: **Details of regression coefficients for thermal parameters of PHP for DI water using 60% FRs at various heat inputs**

Thermal parameters	Heat inputs	a_0	a_1	$a_2 \times 10^{-3}$	$a_3 \times 10^{-5}$
T_c [K]	40 W	0.00	-70.3001	218.1916	-22.4289
	60 W	0.00	-20.4264	61.1650	-5.9470
	80 W	0.00	-1.7451	1.0564	0.4694
	100 W	0.00	1.4241	-8.2066	1.3387
	120 W	0.00	-37.6637	112.0639	-10.9868
P [bar]	40 W	0.00	-0.3665	1.0265	-0.0932
	60 W	0.00	0.5094	-1.7909	0.2085
	80 W	0.00	-0.2711	0.6509	-0.0458
	100 W	0.00	0.5372	-1.8484	0.2113
	120 W	0.00	-0.1473	0.3309	-0.0199
dT [K]	40 W	0.00	71.3001	-218.1916	22.4289
	60 W	0.00	21.4264	-61.1650	-0.4694
	80 W	0.00	2.7451	-1.0564	-0.4694
	100 W	0.00	-0.4241	8.2066	-1.3387
	120 W	0.00	38.6637	-112.0639	10.9868
TR [K/W]	40 W	0.00	1.7825	-5.4548	0.5607
	60 W	0.00	0.3571	-1.0194	0.0991
	80 W	0.00	0.0343	-0.0132	-0.0059
	100 W	0.00	-0.0042	0.0821	-0.0134
	120 W	0.00	0.3222	-0.9339	0.0916

Table 8: **Details of regression coefficients for thermal parameters of PHP for nanofluid using 60% FRs at various heat inputs**

Thermal parameters	Heat inputs	a_0	a_1	$a_2 \times 10^{-3}$	$a_3 \times 10^{-5}$
T_c [K]	40 W	0.00	-48.1599	147.1372	-14.8273
	60 W	0.00	-77.0224	235.0023	-23.7242
	80 W	0.00	18.852	-60.6455	6.6126
	100 W	0.00	-61.082	188.0143	-19.1728
	120 W	0.00	-8.851	23.4898	-1.9180
P [bar]	40 W	0.00	-1.0103	2.9354	-0.2813
	60 W	0.00	0.1288	-0.5626	0.0766
	80 W	0.00	-0.6140	1.8013	-0.1748
	100 W	0.00	-1.4611	4.4070	-0.4415
	120 W	0.00	1.1424	-3.6720	0.3936
dT [K]	40 W	0.00	49.1599	-147.1372	14.8273
	60 W	0.00	78.0224	-235.0023	23.7242
	80 W	0.00	-17.852	60.6455	-6.6126
	100 W	0.00	62.082	-188.0143	19.1728
	120 W	0.00	9.851	-23.4898	1.9180
TR [K/W]	40 W	0.00	1.229	-3.6784	0.3707
	60 W	0.00	1.3004	-3.9167	0.3954
	80 W	0.00	-0.2232	0.7581	-0.0827
	100 W	0.00	0.6208	-1.8801	0.1917
	120 W	0.00	0.0821	-0.1957	0.0160

References

[1] Random forests. *Machine Learning*, 45:5–32, 2001. ISSN 1573-0565. doi: https://doi.org/10.1023/A:1010933404324.

[2] H. Akachi. Structure of a heat pipe, 1990. US Patent 4,921,041.

[3] M. Alhuyi Nazari, M. H. Ahmadi, R. Ghasempour, M. B. Shafii, O. Mahian, S. Kalogirou, and S. Wongwises. A review on pulsating heat pipes: From solar to cryogenic applications. *Applied Energy*, 222:475–484, 2018. ISSN 0306-2619. doi: https://doi.org/10.1016/j.apenergy.2018.04.020. URL `https://www.sciencedirect.com/science/article/pii/S0306261918305634`.

[4] M. Chen and J. Li. Nanofluid-based pulsating heat pipe for thermal management of lithium-ion batteries for electric vehicles. *Journal of Energy Storage*, 32:101715, 2020. ISSN 2352-152X. doi: https://doi.org/10.1016/j.est.2020.101715. URL `https://www.sciencedirect.com/science/article/pii/S2352152X20315528`.

[5] C. Czajkowski, A. I. Nowak, P. Błasiak, A. Ochman, and S. Pietrowicz. Experimental study on a large scale pulsating heat pipe operating at high heat loads, different adiabatic lengths and various filling ratios of acetone, ethanol, and water. *Applied Thermal Engineering*, 165:114534, 2020. ISSN 1359-4311. doi: https://doi.org/10.1016/j.applthermaleng.2019.114534. URL `https://www.sciencedirect.com/science/article/pii/S1359431119332089`.

[6] P. K. Das, N. Islam, A. K. Santra, and R. Ganguly. Experimental investigation of thermophysical properties of al2o3–water nanofluid: Role of surfactants. *Journal of Molecular Liquids*, 237:304–312, 2017. ISSN 0167-7322. doi: https://doi.org/10.1016/j.molliq.2017.04.099. URL `https://www.sciencedirect.com/science/article/pii/S0167732217308516`.

[7] X. Han, X. Wang, H. Zheng, X. Xu, and G. Chen. Review of the development of pulsating heat pipe for heat dissipation. *Renewable and Sustainable Energy Reviews*, 59:692–709, 2016. ISSN 1364-0321. doi: https://doi.org/10.1016/j.rser.2015.12.350. URL `https://www.sciencedirect.com/science/article/pii/S1364032116000034`.

[8] S. Jafarmadar, N. Azizinia, N. Razmara, and F. Mobadersani. Thermal analysis and entropy generation of pulsating heat pipes using nanofluids. *Applied Thermal Engineering*, 103:356–364, 2016. ISSN 1359-4311. doi: https://doi.org/10.1016/j.applthermaleng.2016.03.032. URL `https://www.sciencedirect.com/science/article/pii/S1359431116303246`.

[9] S. Khandekar, N. Dollinger, and M. Groll. Understanding operational regimes of closed loop pulsating heat pipes: an experimental study. *Applied Thermal Engineering*, 23(6):707–719, 2003. ISSN 1359-4311. doi: https://doi.org/10.1016/S1359-4311(02)00237-5. URL `https://www.sciencedirect.com/science/article/pii/S1359431102002375`.

[10] F. K. Kholi, S. Park, J. S. Yang, M. Y. Ha, and J. K. Min. A detailed review of pulsating heat pipe correlations and recent advances using artificial neural network for improved performance prediction. *International Journal of Heat and Mass Transfer*, 207:124010, 2023. ISSN 0017-9310. doi: https://doi.org/10.1016/j.ijheatmasstransfer.2023.124010. URL `https://www.sciencedirect.com/science/article/pii/S0017931023001631`.

[11] W. Kim and S. J. Kim. Effect of a flow behavior on the thermal performance of closed-loop and closed-end pulsating heat pipes. *International Journal of Heat and Mass Transfer*, 149:119251, 2020. ISSN 0017-9310. doi: https://doi.org/10.1016/j.ijheatmasstransfer.2019.119251. URL `https://www.sciencedirect.com/science/article/pii/S0017931019345879`.

[12] Z. Li, M. Sarafraz, A. Mazinani, H. Moria, I. Tlili, T. A. Alkanhal, M. Goodarzi, and M. R. Safaei. Operation analysis, response and performance evaluation of a pulsating heat pipe for low temperature heat recovery. *Energy Conversion and Management*, 222:113230, 2020. ISSN 0196-8904. doi: https://doi.org/10.1016/j.enconman.2020.113230. URL `https://www.sciencedirect.com/science/article/pii/S0196890420307743`.

[13] Y.-H. Lin, S.-W. Kang, and H.-L. Chen. Effect of silver nano-fluid on pulsating heat pipe thermal performance. *Applied Thermal Engineering*, 28(11):1312–1317, 2008. ISSN 1359-4311. doi: https://doi.org/10.1016/j.applthermaleng.2007.10.019. URL `https://www.sciencedirect.com/science/article/pii/S1359431107003468`.

[14] Q. Z. S. S. L. W. Lipeng Wang, Yue Cai and H. Zhan. Heat transfer characteristics of single-ring closed php. *Journal of Mechanical Science and Technology*, 35:1771–1779, 2021. doi: https://doi.org/10.1007/s12206-021-0339-0. URL https://link.springer.com/article/10.1007/s12206-021-0339-0.

[15] J. Loyola-Fuentes, L. Pietrasanta, M. Marengo, and F. Coletti. Machine Learning Algorithms for Flow Pattern Classification in Pulsating Heat Pipes. *Energies*, 15(6):1–20, March 2022. URL https://ideas.repec.org/a/gam/jeners/v15y2022i6p1970-d766671.html.

[16] H. B. Ma, C. Wilson, B. Borgmeyer, K. Park, Q. Yu, S. U. S. Choi, and M. Tirumala. Effect of nanofluid on the heat transport capability in an oscillating heat pipe. *Applied Physics Letters*, 88(14):143116, 2006. doi: 10.1063/1.2192971. URL https://doi.org/10.1063/1.2192971.

[17] M. Mohammadi, M. Mohammadi, A. R. Ghahremani, M. B. Shafii, and N. Mohammadi. Experimental investigation of thermal resistance of a ferrofluidic closed-loop pulsating heat pipe. *Heat Transfer Engineering*, 35(1):25–33, 2014. doi: 10.1080/01457632.2013.810086. URL https://doi.org/10.1080/01457632.2013.810086.

[18] H. Y. Noh and S. J. Kim. Numerical simulation of pulsating heat pipes: Parametric investigation and thermal optimization. *Energy Conversion and Management*, 203:112237, 2020. ISSN 0196-8904. doi: https://doi.org/10.1016/j.enconman.2019.112237. URL https://www.sciencedirect.com/science/article/pii/S0196890419312439.

[19] K. Parmar, A. K. Parwani, and S. Tripathi. A review on recent advances in pulsating heat pipes. In *Recent Advances in Mechanical Infrastructure*, pages 89–96, Singapore, 2022. Springer Nature Singapore. ISBN 978-981-16-7660-4.

[20] V. M. Patel and H. B. Mehta. Channel wise displacement-velocity-frequency analysis in acetone charged multi-turn closed loop pulsating heat pipe. *Energy Conversion and Management*, 195:367–383, 2019. ISSN 0196-8904. doi: https://doi.org/10.1016/j.enconman.2019.05.014. URL https://www.sciencedirect.com/science/article/pii/S0196890419305618.

[21] V. M. Patel, Gaurav, and H. B. Mehta. Influence of working fluids on startup mechanism and thermal performance of a closed loop pulsating heat pipe. *Applied Thermal Engineering*, 110:1568–1577, 2017. ISSN 1359-4311. doi: https://doi.org/10.1016/j.applthermaleng.2016.09.017. URL https://www.sciencedirect.com/science/article/pii/S1359431116316179.

[22] D. E. . L. W. Pierre Geurts. Extremely randomized trees. *Machine Learning*, 63:3–42, 2006. ISSN 1573-0565. doi: https://doi.org/10.1007/s10994-006-6226-1. URL https://link.springer.com/article/10.1007/s10994-006-6226-1.

[23] J. Qu and H. Wu. Thermal performance comparison of oscillating heat pipes with sio2/water and al2o3/water nanofluids. *International Journal of Thermal Sciences*, 50(10):1954–1962, 2011. ISSN 1290-0729. doi: https://doi.org/10.1016/j.ijthermalsci.2011.04.004. URL https://www.sciencedirect.com/science/article/pii/S1290072911001207.

[24] J. Qu, H. ying Wu, and P. Cheng. Thermal performance of an oscillating heat pipe with al2o3–water nanofluids. *International Communications in Heat and Mass Transfer*, 37(2):111–115, 2010. ISSN 0735-1933. doi: https://doi.org/10.1016/j.icheatmasstransfer.2009.10.001. URL https://www.sciencedirect.com/science/article/pii/S0735193309002462.

[25] H. R. Seyf, S. Kim, and Y. Zhang. Thermal performance of an al2o3–water nanofluid pulsating heat pipe. *Journal of Electronic Packaging*, 135, 06 2013. doi: 10.1115/1.4024145.

[26] S. Soni and A. K. Parwani. Experimental study on closed loop oscillating heat pipe for different filling ratios. *IOP Conference Series: Materials Science and Engineering*, 491(1):012019, mar 2019. doi: 10.1088/1757-899X/491/1/012019. URL https://dx.doi.org/10.1088/1757-899X/491/1/012019.

[27] W.-W. Wang, L. Wang, Y. Cai, G.-B. Yang, F.-Y. Zhao, D. Liu, and Q.-H. Yu. Thermo-hydrodynamic model and parametric optimization of a novel miniature closed oscillating heat pipe with periodic expansion-constriction condensers. *International Journal of Heat and Mass Transfer*, 152:119460, 2020. ISSN 0017-9310. doi: https://doi.org/10.1016/j.

ijheatmasstransfer.2020.119460. URL https://www.sciencedirect.com/science/article/pii/S0017931019342152.

[28] A. Wei, J. Qu, H. Qiu, C. Wang, and G. Cao. Heat transfer characteristics of plug-in oscillating heat pipe with binary-fluid mixtures for electric vehicle battery thermal management. *International Journal of Heat and Mass Transfer*, 135:746–760, 2019. ISSN 0017-9310. doi: https://doi.org/10.1016/j.ijheatmasstransfer.2019.02.021. URL https://www.sciencedirect.com/science/article/pii/S0017931018341127.

[29] M. Xing, J. Yu, and R. Wang. Performance of a vertical closed pulsating heat pipe with hydroxylated mwnts nanofluid. *International Journal of Heat and Mass Transfer*, 112:81–88, 2017. ISSN 0017-9310. doi: https://doi.org/10.1016/j.ijheatmasstransfer.2017.04.112. URL https://www.sciencedirect.com/science/article/pii/S0017931016341217.

[30] H. Xu, P. Zhang, L. Yan, D. Xu, W. Ma, and L. Wang. Thermal characteristic and analysis of microchannel structure flat plate pulsating heat pipe with silver nanofluid. *IEEE Access*, 7:51724–51734, 2019. doi: 10.1109/ACCESS.2019.2907820.

[31] Y. Xu, Y. Xue, H. Qi, and W. Cai. Experimental study on heat transfer performance of pulsating heat pipes with hybrid working fluids. *International Journal of Heat and Mass Transfer*, 157:119727, 2020. ISSN 0017-9310. doi: https://doi.org/10.1016/j.ijheatmasstransfer.2020.119727. URL https://www.sciencedirect.com/science/article/pii/S0017931019365974.

[32] H. Yang, S. Khandekar, and M. Groll. Performance characteristics of pulsating heat pipes as integral thermal spreaders. *International Journal of Thermal Sciences*, 48(4):815–824, 2009. ISSN 1290-0729. doi: https://doi.org/10.1016/j.ijthermalsci.2008.05.017. URL https://www.sciencedirect.com/science/article/pii/S1290072908001324.

[33] X. Zhang, Z. Li, L. Luo, Y. Fan, and Z. Du. A review on thermal management of lithium-ion batteries for electric vehicles. *Energy*, 238:121652, 2022. ISSN 0360-5442. doi: https://doi.org/10.1016/j.energy.2021.121652. URL https://www.sciencedirect.com/science/article/pii/S0360544221019009.

[34] Z. Zhou, Y. Lv, J. Qu, Q. Sun, and D. Grachev. Performance evaluation of hybrid oscillating heat pipe with carbon nanotube nanofluids for electric vehicle battery cooling. *Applied Thermal Engineering*, 196:117300, 2021. ISSN 1359-4311. doi: https://doi.org/10.1016/j.applthermaleng.2021.117300. URL https://www.sciencedirect.com/science/article/pii/S1359431121007365.

[35] M. Zufar, P. Gunnasegaran, H. Kumar, and K. Ng. Numerical and experimental investigations of hybrid nanofluids on pulsating heat pipe performance. *International Journal of Heat and Mass Transfer*, 146:118887, 2020. ISSN 0017-9310. doi: https://doi.org/10.1016/j.ijheatmasstransfer.2019.118887. URL https://www.sciencedirect.com/science/article/pii/S0017931019326699.